Ex situ n+ doping of GeSn alloys via non-equilibrium processing

Prucnal, S.; Berencén, Y.; Wang, M.; Rebohle, L.; Böttger, R.; Fischer, I. A.; Augel, L.; Oehme, M.; Schulze, J.; Voelskow, M.; Helm, M.; Skorupa, W.; Zhou, S.;

ACCEPTED MANUSCRIPT

Ex-situ n+ doping of GeSn alloys via non-equilibrium processing

Ex-situ n+ doping of GeSn alloys via non-equilibrium processing

S. Prucnal[1], Y. Berencén[1], M. Wang[1], L. Rebohle[1], R. Böttger [1], I. A. Fischer[2], L. Augel[2], M. Oehme[2], J. Schulze[2], M. Voelskow[1], M. Helm[1,3], W. Skorupa[1] and S. Zhou[1]

[1]Helmholtz-Zentrum Dresden-Rossendorf, Institute of Ion Beam Physics and Materials Research, Bautzner Landstrasse 400, 01328 Dresden, Germany

[2]University of Stuttgart, Institute of Semiconductor Engineering and Research Center SCoPE, Stuttgart, Germany

[3]Center for Advancing Electronics Dresden (cfaed), Technische Universität Dresden, 01062 Dresden, Germany

Abstract

Full integration of Ge-based alloys like GeSn with complementary-metal-oxide-semiconductor (CMOS) technology would require the fabrication of p- and n-type doped regions for both planar and tri-dimensional device architectures which is challenging using *in-situ* doping techniques. In this work, we report on the influence of the *ex-situ* doping on the structural, electrical and optical properties of GeSn alloys. n-type doping is realized by P implantation into GeSn alloy layers grown by molecular beam epitaxy (MBE) followed by flash lamp annealing (FLA). We show that the effective carrier concentration up to 1×10^{19} cm^{-3} can be achieved without affecting the Sn distribution. A Sn segregation at the surface accompanied with a Sn diffusion towards the crystalline/amorphous GeSn interface is found at P fluences higher than 3×10^{15} cm^{-2} and electron concentration of about 4×10^{19} cm^{-3}. Optical and structural properties of ion-implanted GeSn layers are comparable with the *in-situ* doped MBE grown layers.

Keywords: GeSn, MBE, flash lamp annealing, ion implantation, n-type doping

1

1. Introduction

Germanium is the most promising material to be fully integrated with silicon technology. Both the hole and electron mobilities in Ge are much higher than in silicon. The small separation of only 134 meV between the direct band gap at the Γ point and the indirect band gap at the L point gives the possibility to convert Ge from an indirect to a direct band gap material [1-3]. This approach can be realized by: (i) ultra-high n-type doping, (ii) introducing biaxial tensile strain and (iii) alloying with Sn [4-9]. The n-type Ge becomes a direct band gap material for an electron concentration higher than 8×10^{19} cm^{-3}. At such high doping levels Ge is strongly degenerated with the Fermi energy located high in the conduction band (CB). At room temperature (RT) the L valley is fully filled with electrons, which allows to populate the Γ valley with thermal-energy electrons. As the Fermi energy is located above the minimum of the Γ valley, direct radiative recombination between electrons in the Γ valley and holes in the valence band (VB) takes place. This is experimentally evidenced by the increase of the photoluminescence (PL) intensity with increasing temperature [6]. Ultra-high n-type Ge is however metastable and during post-growth annealing, e.g. during ohmic contact formation, the effective carrier concentration will be reduced to the equilibrium level of about $2-3 \times 10^{19}$ cm^{-3} [9]. Kimerling's group has shown that the minimum electron concentration required for Ge to become a quasi-direct band gap material can be significantly reduced by the combination of n-type doping with biaxial tensile strain [6]. Simultaneously, the biaxial tensile strain can also be reduced much below 1.9%, which is required for the formation of a direct band gap in intrinsic Ge [10]. Recently, much more effort has been made on the fabrication of direct band gap Ge *via* Sn alloying. In biaxial tensile strained GeSn alloy a direct band gap can be achieved at a Sn content as low as 6%. It has also been shown that the direct band gap GeSn alloy with a Sn content in the range of 10% can be used as lasing material operating at low temperatures in the mid-infrared range [11-13].

The equilibrium solid solubility of Sn in Ge is below 1% and the lattice mismatch between α-Sn and Ge is about 14.7%. The lattice mismatch between direct band gap GeSn with 10% of Sn and Ge lies in the range of 1.5%. The growth of high quality GeSn alloys can be realized by non-equilibrium processing like molecular beam epitaxy (MBE) [14] and ion implantation followed by non-equilibrium thermal annealing using FLA [15]. The GeSn layers are usually grown on so-called "virtual substrates" placed on a Si wafer where the buffer layer is used to annihilate misfit dislocations and reduce the strain. During the epitaxial regrowth of an implanted layer the *in-plane* lattice parameter is preserved. The lattice parameter of relaxed

2

GeSn increases with increasing the Sn concentration and it is bigger than that of relaxed Ge. Therefore, the GeSn layers made by ion implantation and post implantation annealing are compressively strained.

The MBE growth of GeSn on Si is performed at extremely low temperature, therefore, *in-situ* ultra-high doping of GeSn alloys is challenging. This can be overcome by combining the ion implantation followed by nonequilibrium thermal processing with MBE grown intrinsic or lightly doped GeSn alloys. During the recent years, FLA has reached a high level of interest as an annealing method in the ms-range for many purposes, especially driven by the needs of advanced semiconductor processing, see Refs. 16, 17, 18 for recent reviews, and more specific, also those of germanium-based materials research: shallow junctions [19], nanoclusters [20], advanced processing [21, 22] etc.

In this work, we investigate the influence of P ion implantation followed by ms-range FLA on the redistribution of Sn in MBE grown GeSn alloy with 5% of Sn. We found that the Sn distribution along the GeSn layer is not affected for effective doping levels up to 1×10^{19} cm^{-3}. However, Sn atoms start diffusing towards both the surface of the GeSn:P layer and the crystalline/amorphous interface at P concentrations higher than 2×10^{19} cm^{-3}. Additionally, the formation of ohmic contacts to heavily doped n-type GeSn is demonstrated together with the electrical activation of P by the diffusion of Ni atoms into the P-implanted GeSn layers during a single-step FLA for 3 ms. Finally, we investigate the reflectivity of the doped layers and find a room-temperature plasma frequency as high as 1400 cm^{-1} for *ex-situ* doped GeSn and about 1700 cm^{-1} for *in-situ* doped GeSn alloys, which makes the material suitable for mid-infrared plasmonics.

2. Experimental part

Two samples with 300 nm thick layers of Ge$_{0.95}$Sn$_{0.05}$ were grown by MBE on (100) 4-inch p$^-$ Si substrates (N$_A$ ~ 10^{15} cm^2). One sample only contained the non-intentional background doping, the other was *in-situ* doped using Sb as a dopant. For both samples the growth process started with the deposition of a 50 nm Si-layer at a substrate temperature of 600° C followed by the deposition of the GeSn films with a nominal thickness of 300 nm at substrate temperatures of 160°C. The dopant fluxes to attain the doping concentration of 5×10^{19} cm^{-3} in the *in-situ* doped layers were pre-calibrated in Si using four-point probe and secondary ion mass spectroscopy measurements. Using the unintentionally doped GeSn layer, five samples (GeSn:P_1 to GeSn:P_5) were implanted with P ions at an energy of 80 keV and different fluences in the range of 3×10^{14} to 9×10^{15} cm^{-2}, see Table 1. The thickness of the P-doped

3

layer is about 120 nm. During the ion implantation process the sample holder was kept at liquid nitrogen temperature. To keep the temperature of the GeSn surface during ion implantation below -20 ^{o}C (to avoid the heating effect of the implanted surface by incident ions), the ion flux was reduced to 1 μA/cm^2 and below.

Table 1. Carrier concentration of as-grown and *ex-situ* doped GeSn layers annealed for 3 ms using FLA with an energy density of 58 Jcm^{-2}. Prior to FLA the samples were preheated at the temperature of 180 ^{o}C for 30 s. The *in-situ* doped sample was annealed at 65 Jcm^{-2} for 3 ms without preheating. The ion fluence was determined taking into account the uncertainty associated to the ion implantation system which is close to 5%. The carrier concentration and the carrier mobility measured by Hall effect are obtained with an uncertainty of around 2%.

Sample	Dopant	Implantation/Doping parameters			FLA parameters	
		Fluence/concentration (cm^{-2}) / (cm^{-3})	Carrier concentr. (cm^{-3})	Carrier mobility (cm^{2}V^{-1}s^{-1})	Energy density (Jcm^{-2})	Pre-heating
GeSn_1	no	-/ -	5.7×10^{17} (p-type)	155±3	65 ± 1	no
GeSn:P_1	P	3×10^{14}/2.5×10^{19}	2.20±0.04×10^{18}	190±4	58 ± 1	yes
GeSn:P_2	P	9×10^{14}/7.5×10^{19}	2.20±0.04×10^{19}	246±5	58 ± 1	yes
GeSn:P_3	P	3×10^{15}/2.5×10^{20}	3.80±0.07×10^{19}	255±5	58 ± 1	yes
GeSn:P_4	P	6×10^{15}/5.0×10^{20}	4.20±0.08×10^{19}	263±5	58 ± 1	yes
GeSn:P_5	P	9×10^{15}/7.5×10^{20}	4.50±0.08×10^{19}	282±6	58 ± 1	yes
GeSn:Sb	Sb	− /5.0×10^{19}	5.00±0.10×10^{19}	110±2	65 ± 1	no

Prior to the ion implantation, a 30 nm thick SiO$_2$ capping layer was deposited by plasma enhanced chemical vapor deposition. Both the low-temperature ion implantation and the SiO$_2$ capping layer prevent the GeSn surface from sputtering and roughening commonly observed in Ge after ion irradiation [23]. Millisecond-flash lamp annealing was used to electrically activate the implanted P atoms and in turn to repair the damaged crystal structure of GeSn upon ion implantation. The annealing process was performed from the rear side of the wafer for all samples [22]. We have previously shown that the conventional FLA approach from the front side causes only a partial epitaxial regrowth of the implanted Ge and the formation of a polycrystalline Ge layer at the surface [21, 24]. After optimization of the annealing parameters the implanted samples were annealed for 3 ms at an energy density of 58±1 Jcm^{-2} with a preheating step at a temperature of 180°C for 30 s performed with halogen lamps. Not-implanted and *in-situ* doped samples were also annealed for 3 ms at an energy density of 65±1

4

Jcm^{-2} without preheating. The different parameters were chosen after it had been found that pre-heating leads to a considerable reduction in measured dopant concentration in the *in-situ* doped sample. After annealing the capping layer was removed with buffered hydrofluoric acid solution. As a result, an about 120 nm thick n-type GeSn layer was achieved. The Sn distribution in the as-grown and implanted layer was investigated by random and channelling Rutherford backscattering spectrometry (RBS/R and RBS/C). The RBS was performed using the 1.7 MeV He^{+} beam of the Rossendorf van de Graff accelerator. The He^{+} beam was focused on the 1 mm diameter spot. The strain evolution and the change of Sn composition in the near-surface region in implanted and annealed samples were investigated using micro-Raman spectroscopy. The phonon spectra were determined by micro-Raman spectroscopy in backscattering geometry in the range of 100 to 600 cm^{-1} using a 532 nm Nd:YAG laser with a liquid-nitrogen cooled charge-coupled device camera. The Fourier-transform infrared spectroscopy (FTIR) measurements were performed at RT using a Bruker Vertex 80v FT-IR system. The simulation of the dielectric function was carried out with a multilayer model based on transfer matrix method. The effective carrier concentration in the investigated GeSn layers was determined from low-temperature Hall effect data. Hall measurements were performed in a van der Pauw configuration using a commercial Lakeshore Hall System HMS 9709A in the temperature range from 2.5 to 300 K. Subsequently, ohmic contacts were made using 10 nm thick Ni deposited on the as-implanted sample and *in-situ* Ni diffusion into the n-type GeSn layer. In this case both the Ni diffusion and P activation take place during the same single FLA treatment. The measurement of the contact resistance was carried out using the transfer length method (TLM). 200 μm long × 50 μm wide Ni stripes separated by 10, 20, 40, 60, 80 and 100 μm were deposited on Ge using optical lithography and a lift-off step. The TLM structures allowed us to extract the contact resistance (R_c), the transfer length (L_T), and the sheet resistance (R_s) from which the specific contact resistance (ρ_c) is subsequently calculated.

## 3. Results and discussion

3.a. Structural properties of *ex-situ* doped GeSn

The Sn redistribution in the as-grown and the P-implanted GeSn layers after FLA was investigated by RBS C/R spectrometry. Since the results show qualitative differences for the samples implanted at lower fluences (3×10^{14} and 9×10^{14} cm^{-2}) compared to the samples

implanted at higher fluences (3×10^{15}, 6×10^{15} and 9×10^{15} cm^{-2}), those two groups of samples will be discussed separately.

The random spectra from the implanted and the not-implanted samples are the same and denoted as RBS/R. The preheating performed prior to the FLA step at 180 $^{\circ}$C for 30s was found to have no influence on the Sn distribution. Therefore, the RBS spectra obtained from the as-preheated samples are not shown. Even the lowest implantation fluence is sufficiently high to introduce a significant defect concentration which converts the implanted layer from single crystalline to quasi-amorphous (see Fig. 1a). The threshold fluence for amorphization of Ge or GeSn *via* P ions at room temperature is in the range of 5×10^{14} cm^{-2} [25]. The ion implantation itself does not affect the Sn distribution within the layer (see Fig. 1a) and the P-doped layer is of about 120 nm thick. Also FLA does not affect the Sn distribution for the low P-fluences (see Fig. 1a). The yield in the channeling direction is below 10% of that of the random direction confirming a full recrystallization of the implanted layer *via* solid phase epitaxy. Figure 1b shows the random and channeling RBS spectra obtained from the flash lamp annealed not-implanted sample and channeling spectra obtained from the implanted and the annealed samples (lower fluences).
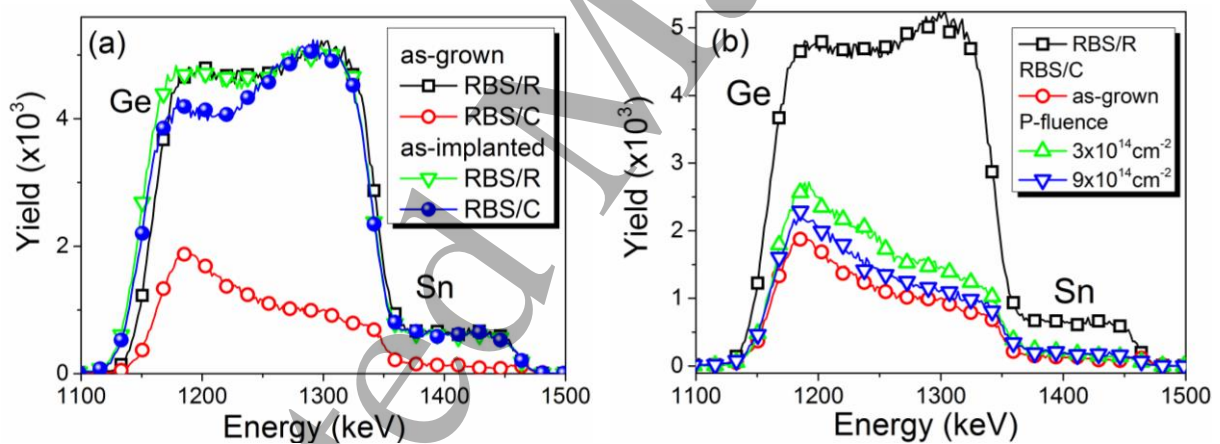
Figure 1. RBS random and channelling spectra obtained from the as-grown sample (GeSn_1) as well as samples GeSn:P_1 (P fluence of 3×10^{14} cm^{-2}) and GeSn:P_2 (P fluence of 9×10^{14} cm^{-2}). (a) A comparison of RBS/R and RBS/C spectra from GeSn_1 and GeSn:P_1 prior to FLA clearly shows that the implanted layer is quasi-amorphous. (b) FLA induces a full recrystallization of the implanted layers as shown by the drastic reduction in yield for the RBS channelling spectra of samples GeSn:P_1 and GeSn:P_2.

Figure 2a shows the random RBS spectra obtained from the GeSn annealed and implanted samples with the high P fluence. Ion implantation does not cause any redistribution of Sn irrespective of the used P fluence. However, in these samples, we found that during FLA Sn

diffuses towards the surface and the amorphous/crystalline interface. The diffusion of Sn increases with increasing P fluence (see Fig. 2c). The Sn redistribution after high fluence ion implantation and FLA was calculated based on the RBS data using RUMP Software. It was shown that the diffusion of Sn is mediated by vacancies and depends on the Fermi level position relative to the band gap and on the charging state of vacancies [26, 27]. The energy activation for diffusion of Sn atoms in Ge is in the range of 2.48 – 3.65 eV and strongly depends on the type and level of doping [26]. P implantation causes the formation of vacancies and the Fermi energy moves towards the CB minimum together with increasing electrical activation of P during annealing [28, 29]. Moreover, n-type dopants in Ge similar to Sn are fast diffusers having a low solid solubility. It was proposed that Sn co-doping would help to decrease the diffusion of n-type dopants and both Sn and P would be trapped at their initial positions [30].
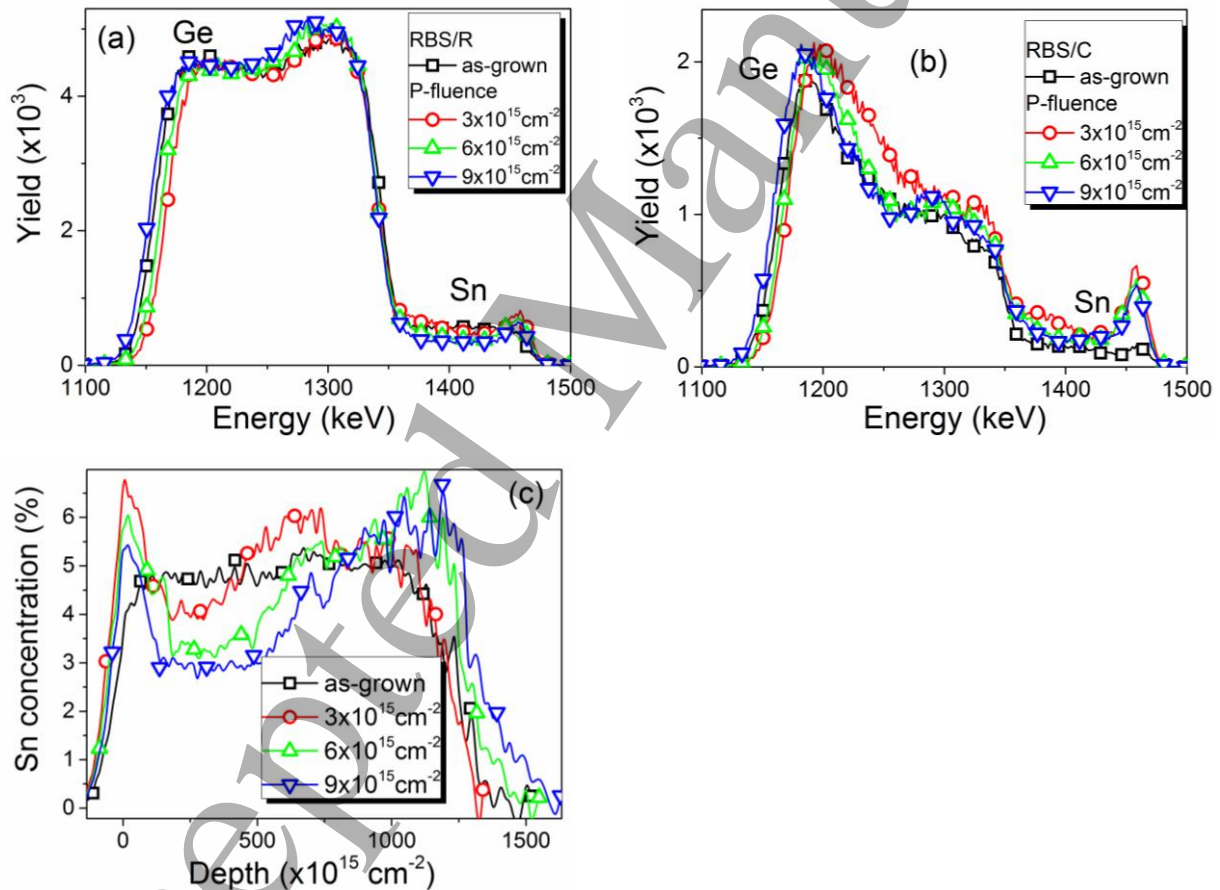

Figure 2. RBS random direction spectra (a) channelling spectra recorded from highly P doped GeSn after FLA for 3 ms (b) and Sn distribution (c).

In our case, for the highest P fluence the GeSn layer is strongly degenerate with the Fermi energy lying above the CB minimum. The diffusion of Sn increases with increasing vacancy

7

and electron concentrations. Finally, strong segregation of Sn at the surface takes place. This also is confirmed by RBS channelling spectra, where a strong peak at a channel number of about 840 is clearly visible (see Fig 2b).

3.b Optical properties of *ex-situ* doped GeSn

Raman spectroscopy is non-destructive and a very sensitive method to investigate the strain and the composition of Ge based alloys. Assuming a fully relaxed GeSn film the Sn content x_{Sn} in GeSn can be determined by the shift of the longitudinal optical (LO) phonon mode with respect to undoped Ge ($\Delta\omega$) [31] according to

$$\Delta\omega = \omega_{GeSn} - \omega_{Ge} = c \times x_{Sn} \qquad (1).$$

Similarly, the *in-plane* strain ε can be measured and calculated from the Raman spectra for a given Sn content in strained GeSn alloys according to

$$\Delta\omega = a \times x_{Sn} + b \times \varepsilon \qquad (2)$$

Various values for the parameters a, b and c have been reported in the literature, we refer to Ref. [32] for recent results. Here, we use a=-83.11, b=-374.53 and c=-82.8 from Ref. 31. We note that the excitation wavelength of the Raman laser corresponds to a penetration depth of ~50 nm in Ge, i.e. our Raman measurements can probe only the surface of the GeSn layers. Similar to RBS, the obtained Raman spectra can be divided into two parts: the low fluence and the high fluence implanted GeSn layers.
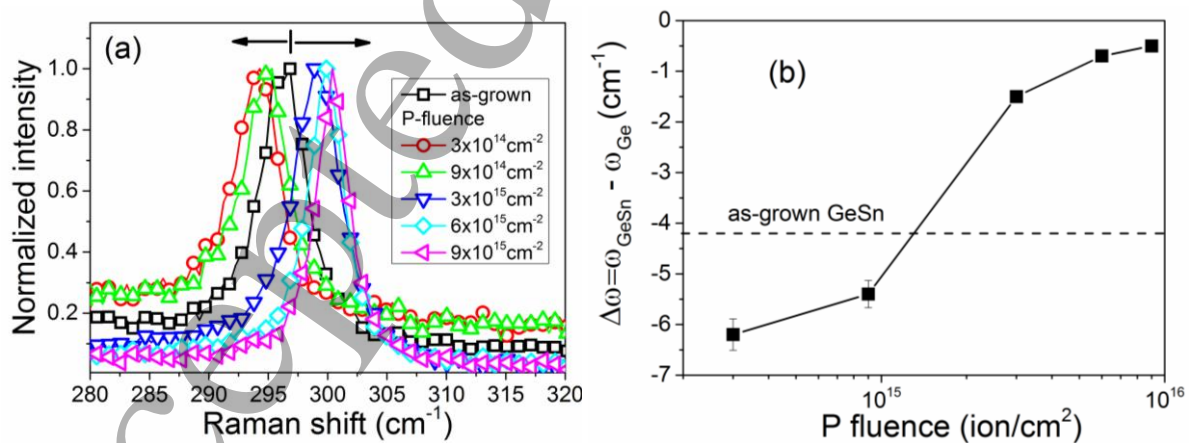

Figure 3. Normalized micro-Raman spectra of P implanted and annealed GeSn films (a). The LO phonon mode shifts as a function of P fluence (b).

According to RBS data the Sn atom distribution is homogeneous for the low fluence implanted GeSn layers. Hence, we assume that the shift of the LO phonon mode in the Raman spectra is due to the strain evolution in the doped and annealed layer. For the highly doped samples a strong segregation of Sn at the surface and diffusion of Sn towards the amorphous/crystalline interface is observed. Therefore, in heavily doped samples the shift of the LO phonon mode can be expected to be caused by changes in composition and strain of the implanted layers. Figure 3b shows the shift of the LO phonon mode as a function of P fluence. The as-grown sample is slightly tensile strained with an *in-plane* biaxial strain of ε=0.012%. After low fluence P implantation followed by FLA, the top layer becomes tensile strained with ε=0.6%. For the highly doped GeSn film the top layer is compressively strained. According to RBS data the average Sn concentration within the implanted layer decreases from 5% to about 3% for the highest P fluence. Knowing the Sn content in the highly doped layer and the peak position of the LO phonon mode for a fully relaxed GeSn layer with a certain Sn content allows us the calculation of the strain [32]. The strain and the Sn composition are summarized in Table 2.

Table 2. Sn composition and strain in P implanted GeSn after FLA determined from RBS and micro-Raman measurements, respectively. The positive and negative strain values correspond to tensile and compressive strain, respectively. The associated uncertainty to these values was found to be of around 5%.

Sample	Dopant	Fluence/concentration (cm^{-2}/cm^{-3})	Energy density (Jcm^{-2})	Sn (%)	$\Delta\omega$ relaxed	$\Delta\omega$ exp.	Strain (%)
GeSn_1	no	-	65 ± 1	5.0±0.1	-4.14	-4.2	0.01±5×10^{-4}
GeSn:P_1	P	3×10^{14}/2.5×10^{19}	58 ± 1	5.0±0.1	-4.14	-6.2	0.54±0.03
GeSn:P_2	P	9×10^{14}/7.5×10^{19}	58 ± 1	5.0±0.1	-4.14	-5.4	0.33±0.02
GeSn:P_3	P	3×10^{15}/2.5×10^{20}	58 ± 1	4.5±0.1	-3.76	-1.5	-0.60±0.03
GeSn:P_4	P	6×10^{15}/5×10^{20}	58 ± 1	3.6±0.1	-2.98	-0.7	-0.60±0.03
GeSn:P_5	P	9×10^{15}/7.5×10^{20}	58 ± 1	3.1±0.1	-2.56	-0.5	-0.55±0.03

3c. Electrical properties

The as-grown sample is p-type with an average carrier concentration in the range of 2×10^{18} cm^{-3} which is reduced to 5.7×10^{17} cm^{-3} after FLA. The p-type conductivity of the non-

9

intentionally doped layer is due to the point defects generated within the film during the MBE growth process at extremely low temperature. These defects mainly consist of Ge and Sn vacancies and/or Sn-vacancy complexes that act as shallow acceptors [33]. We assume that the post-growth sub-second annealing significantly reduces the concentration of vacancies without affecting the Sn distribution. To achieve the n-type doping of GeSn layers the electrically active P concentration must be higher than the concentration of vacancies. In pure Ge the activation efficiency of P is close to 100% for a P concentration below 2×10^{20} cm^{-3} [22]. In ion implanted GeSn layers P atoms can be electrically deactivated via the formation of complex defects with Sn and with vacancies [34]. Therefore, for the formation of n-type GeSn the minimum P concentration must be one order of magnitude higher than the concentration of vacancies. For the middle fluence of P (3×10^{15} cm^{-2}) the electrically active fraction of P is in the range of 20%, but for the highest fluence the activation efficiency drops down to about 5% which can be due to P-P dimer formation like in Ge [16, 22, 35]. In the case of *in-situ* doped GeSn with Sb the effective carrier concentration is hardly affected by the post-grown annealing. But the carrier mobility in P implanted samples is almost tree times higher than in the *in-situ* doped (282 *vs.* 110 cm^{2}V^{-1}s^{-1}). The data obtained at room temperature are summarized in Table 1.
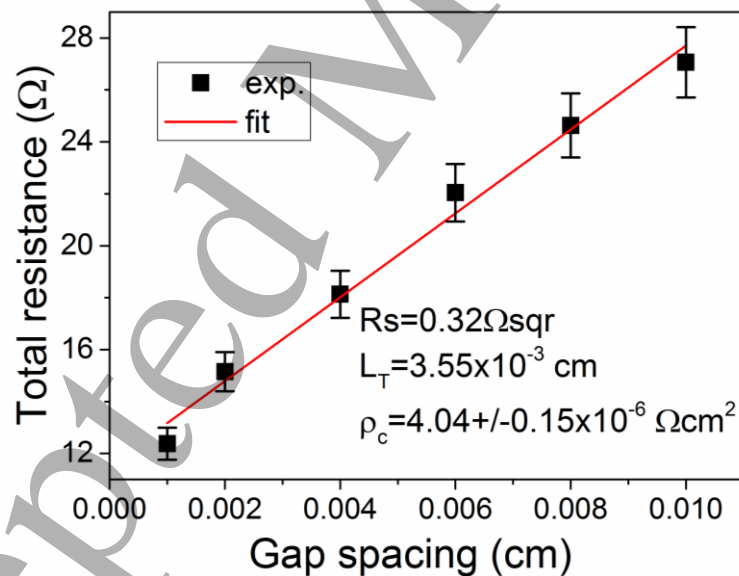

Figure 4. The total resistance as a function of gap spacing derived from TLM for the GeSn sample doped with P at a fluence of 9×10^{15} cm^{-2} followed by FLA for 3 ms.

Figure 4 shows the typical dependence between the total resistance and the gap spacing derived from the transfer length method (TLM) of samples after *in-situ* germanidation for 3

ms at an energy density of the flash lamp of 58 Jcm^{-2}. A nickel-germanide (NiGe) compound was created on the sample doped with a P fluence of 3×10^{15} cm^{-2} which corresponds to a doping level of 3.8×10^{19} cm^{-3}. Importantly, the NiGe layer is formed together with the P activation during the same single FLA step. The formation of ohmic contacts between NiGe and n-type GeSn is confirmed by the linear behaviour of the current-voltage characteristics measured among neighbouring contacts (not shown). To extract the specific contact resistance ρ_c, data points presented in Fig. 4 were linearly fitted to deduce the transfer length L_T and the contact resistance R_C. The sheet resistance (R_{Sh}) and ρ_c are respectively calculated by the following expressions: $R_{Sh} = \frac{R_C W}{L_T}$, and $\rho_C = R_{Sh} L_T^2$, where W is the length of the Ni-germanide stripes (here 200 μm). The resulting R_{sh} and ρ_c were found to be 0.32 Ωsq and $4.04\pm0.15\times10^{-6}$ Ωcm^2, respectively. The specific contact resistivity compares well to $\rho_c = 6.4 \pm 1.5 \times 10^{-4}$ Ωcm^2 obtained for Ni deposited on Ge$_{0.955}$Sn$_{0.045}$ ($N_D = 2 \times 10^{18}$ cm^{-3}) after annealing [36] and $\rho_c = 5.68 \pm 0.17 \times 10^{-6}$ Ωcm^2 obtained for Ni deposited on Ge$_{0.94}$Sn$_{0.06}$ ($N_D = 1.6 \times 10^{19}$ cm^{-3}) without annealing [37].

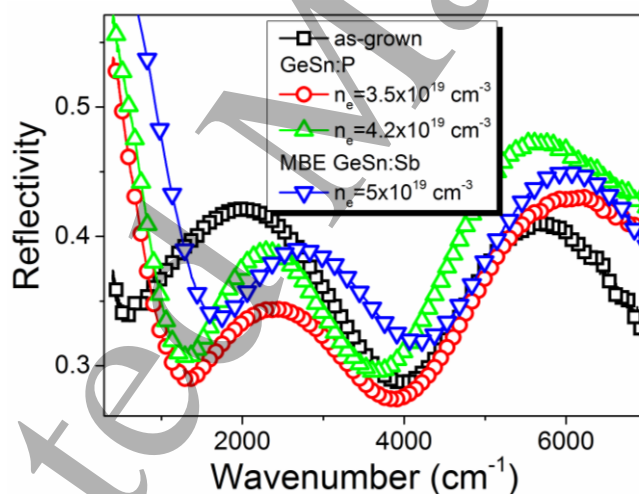**3d. n$^+$ GeSn alloys for mid-infrared plasmonics**.

Figure 5. Reflectivity spectra obtained from not implanted GeSn, P-doped GeSn followed by FLA and *in-situ* Sb doped GeSn.

The heavily P implanted GeSn has an average effective carrier concentration in the range of 5×10^{19} cm^{-3}. Highly n-type doped group-IV semiconductors Ge and GeSn are particularly interesting materials for mid-infrared plasmonic applications which cannot be realized using conventional plasmonic materials like metals [8, 38]. Figure 5 shows the room temperature reflectivity as a function of the wavenumber of the incident light for an un-doped GeSn film, a P implanted layer and an *in-situ* Sb doped GeSn with a similar active carrier concentration in

11

the range of 5×10^{19} cm^{-3}. In all cases the GeSn layer is 300 nm thick. The main difference between *ex-situ* and *in-situ* doped GeSn is the thickness of the n^{++}-type layer. To determine the plasma frequency, the experimental FTIR reflectance spectra were fitted using an anisotropic general oscillator layer model composed of a Drude component. In the case of *in-situ* doped sample whole 300 nm thick layer is doped with Sb while in the *ex-situ* doped samples only the top 120 nm layer is implanted with P. The spectra were obtained by FTIR spectroscopy at room temperature. This strongly affects the maximum plasma frequency edge ω, which should be directly proportional to $n_e^{0.5}$ and to $(m^*)^{-0.5}$, where n_e and m* are the effective carrier concentration and the electron effective mass, respectively. If the thickness of the n-type layer is thinner than 300 nm the layer becomes semi-transparent for the incident mid-infrared light like in our case. Even so, the plasma frequency of the implanted layer (1400 cm^{-1}) is close to that of the MBE grown layer *in-situ* doped with Sb (1700 cm^{-1}).

4. Conclusions

We have shown that the GeSn layers can be *ex-situ* doped using non-equilibrium processing i.e. ion implantation and FLA. This allows to fabricate planar devices with different functionalities. An effective carrier concentration in the range of 2×10^{19} cm^{-3} is achieved without affecting the Sn distribution. For the very heavily doped GeSn the Sn diffusion is mediated by vacancies generated by P implantation. The P-doped GeSn layers were demonstrated to be suitable for the mid-infrared plasmonics that can be used to fabricate detectors for controlling the air pollution by greenhouse gases responsible for the global warming.

5. Acknowledgement

6. References:

1. Camacho-Aguilera R, Han Z, Cai Y, Kimerling L C and Michel J 2013 *Appl. Phys. Lett.* **102**, 152106.

2. Zaima S, Nakatsuka O, Taoka N, Kurosawa M, Takeuchi W and Sakashita M 2015 *Sci. Technol. Adv. Mater.* **16**, 043502.

3. Prucnal S, Frigerio J, Napolitani E, Ballabio A, Berencén Y, Rebohle L, Wang M, Böttger R, Voelskow M, Isella G, *et al.* 2017 *Semicond. Sci. Technol.* **32**, 115006.

4. Saito S, Al-Attili A Z, Oda K and Ishikawa Y 2016 *Semicond. Sci. Technol.* **31**, 043002.

5. Liu J, Kimerling L C and Michel J 2012 *Semicond. Sci. Technol.* **27**, 094006.

6. Liu J, Sun X, Pan D, Wang X, Kimerling L C, Koch T L and Michel J 2007 *Opt. Express* **15**, 11272–7.

7. Biswas S, Doherty J, Saladukha D, Ramasse Q, Majumdar D, Upmanyu M, Singha A, Ochalski T, Morris M A and Holmes J D 2016 *Nat Commun.* **7**, 11405.

8. Augel L, Fischer I A, Hornung F, Dressel M, Berrier A, Oehme M and Schulze J 2016 *Opt. Letters* **41**, 4398.

9. Milazzo R, Impellizzeri G, Piccinotti D, De Salvador D, Portavoce A, La Magna A, Fortunato G, Mangelinck D, Privitera V, Carnera A and Napolitani E 2017 *Appl. Phys. Lett.* **110**, 011905.

10. El Kurdi M, Fishman G, Sauvage S and Boucaud P 2010 *J. Appl. Phys.* **107**, 013710.

11. Stange D, Wirths S, von den Driesch N, Mussler D, Stoica T, Ikonic Z, Hartmann J M, Mantl S, Grützmacher D and Buca D 2015 *ACS Photonics*, **2**, 1539−1545.

12. Wirths S, Geiger R, von den Driesch N, Mussler G, Stoica T, Mantl S, Ikonic Z, Luysberg M, Chiussi S, Hartmann J M, *et al.,* 2015 *Nat. Photon.*, **9**, 88–92.

13. Gassenq A, Milord L, Aubin J, Guilloy K, Tardif S, Pauc N, Rothman J, Chelnokov A, Hartmann J M, Reboud V and Calvo V 2016 *Appl. Phys. Lett.* **109**, 242107.

14. Oehme M, Kostecki K, Schmid M, Oliveira F, Kasper E, Schulze J 2014 *Thin Solid Films*, **557**, 169.

15. Gao K, Prucnal S, Huebner R, Baehtz C, Skorupa I, Wang Y, Skorupa W, Helm M and Zhou S 2014 *Appl. Phys. Lett.* **105**, 042107.

13

16. Prucnal S, Rebohle L and Skorupa W 2017 *Mater. Sci. Semicond. Process*, **62**, 115-127.

17. Rebohle L, Prucnal S and Skorupa W, *Semicond. Sci. Technol.* **31**, 103001 (2016).

18. Skorupa W, Schumann T and Rebohle L 2017 *Surface & Coatings Technology* **314**, 169-176.

19. Simoen E, Schaekers M, Liu J, Luo J, Zhao C, Barla K and Collaert N 2016 *Phys. Status Solidi A* **213**, 2799–2808.

20. von Borany J, Grötzschel R, Heinig K-H, Markwitz A, Schmidt B, Skorupa W and Thees H-J 1999 *Solid-State Electronics* **43**, 1159-1163.

21. Wündisch C, Posselt M, Schmidt B, Heera V, Schumann T, Mücklich A, Grötzschel R, Skorupa W, Clarysse T, Simoen E and Hortenbach H 2009 *Appl. Phys. Lett.* **95**, 252107.

22. Prucnal S, Liu F, Voelskow M, Vines L, Rebohle L, Lang D, Berencén Y, Andric S, Boettger R, Helm M *et al.,* 2016 *Sci. Rep.* **6**, 27643.

23. Böttger R, Keller A, Bischoff L and Facsko S 2013 *Nanotechnology* **24** 115702.

24. Heera V, Mücklich A, Posselt M, Voelskow M, Wündisch C, Schmidt B, Skrotzki R, Heinig K H, Herrmannsdörfer T and Skorupa W 2010 *J. Appl. Phys.* **107**, 053508.

25. Koffel S, Scheiblin P, Claverie A and Benassayag G 2009 *J. Appl. Phys.* **105**, 013528 (2009).

26. Tahini H, Chroneos A, Grimes R W and Schwingenschlögl U 2011 *Appl. Phys. Lett.* **99**, 162103.

27. Panayiotatos Y, Saltas V, Chroneos A and Vallianatos F 2017 *J Mater Sci: Mater Electron.* **28**, 9936–9940. DOI 10.1007/s10854-017-6751-7

28. Satta A, Janssens T, Clarysse T, Simoen E, Meuris M, Benedetti A, Hoflijk I, De Jaeger B, Demeurisse C and Vandervorst W W 2006 *J. Vac. Sci. Technol. B* **24**, 494.

29. Bracht H, Schneider S and Kube R 2011 *Microelectron. Eng.*, **88**, 452-457 (2011).

14

30. Tahini H A, Chroneos A, Grimes R W, Schwingenschlögl U and Bracht H 2013 *Phys. Chem. Chem. Phys.,* **15**, 367-371.

31. Cheng R, Wang W, Gong X, Sun L, Guo P, Hu H, Shen Z, Han G and Yeo *Y-C 2013 ECS J. Solid State Sci. Technol.*, **2,** P138-P145.

32. Gassenq A, Milord L, Aubin J, Pauc N, Guilloy K, Rothman J, Rouchon D, Chelnokov A, Hartmann J M, Reboud V and Calvo V 2017 *Appl. Phys. Lett.* **110**, 112101.

33. Prucnal S, Liu F, Berencén Y, Vines L, Bischoff L, Grenzer J, Andric S, Tiagulskyi S, Pyszniak K, Turek M, et al., 2016 *Semicond. Sci. Technol.* **31**, 105012.

34. D'Costa V R, Wang L, Wang W, Lim S L, Chan T K, Chua L H, Henry T, Zou W, Hatem C, Osipowicz T *et al.,* 2014 *Appl. Phys. Lett.* **105**, 122108.

35. Mattoni G, Klesse W M, Capellini G, Simmons M Y and Scappucci G 2013 *ACS Nano* **7**, 11310–11316.

36. Li H, Cheng H H, Lee L C, Lee C P, Su L H and Suen Y W 2014 *Appl. Phys. Lett.* **104**, 241904.

37. Srinivasan V S S, Fischer I A, Augel L, Hornung A, Koerner R, Kostecki K, Oehme M, Rolseth E and Schulze J 2016 *Semicond. Sci. Technol.* **31** 08LT01.

38. Biagioni P, Frigerio J, Samarelli A, Gallacher K, Baldassarre L, Sakat E, Calandrini E, Millar R W, Giliberti V, Isella G, *et al.,* 2015 *J. Nanophotonics*, **9**, 093789.

15